Electronic Supplementary Information (ESI)

Enhancing electrocatalytic nitrogen reduction to ammonia with rare earth (La, Y, Sc) on high-index faceted platinum alloy concave nanocubes

Yu-Jie Mao,‡[a] Feng Liu,‡[a] You-Hu Chen,[b] Xin Jiang,[a] Xin-Sheng Zhao,[a] Tian Sheng,*[c] Jin-Yu Ye,[b] Hong-Gang Liao,[b] Lu Wei,*[a] Shi-Gang Sun*[b]

[a] *School of Physics and Electronic Engineering, Jiangsu Normal University, Xuzhou 221116, China*

[b] *State Key Lab of PCOSS, College of Chemistry and Chemical Engineering, Xiamen University, Xiamen 361005, China*

[c] *College of Chemistry and Materials Science, Anhui Normal University, Wuhu 241000, China*

** Corresponding authors*

E-mail addresses: lwei057@jsnu.edu.cn (L. Wei), sgsun@xmu.edu.cn (S. Sun), tsheng@ahnu.edu.cn (T. Sheng)

‡ *These authors contributed equally to this work.*

1. Electrodeposition behaviors of Pt and rare earth metals in ChCl-U based DES

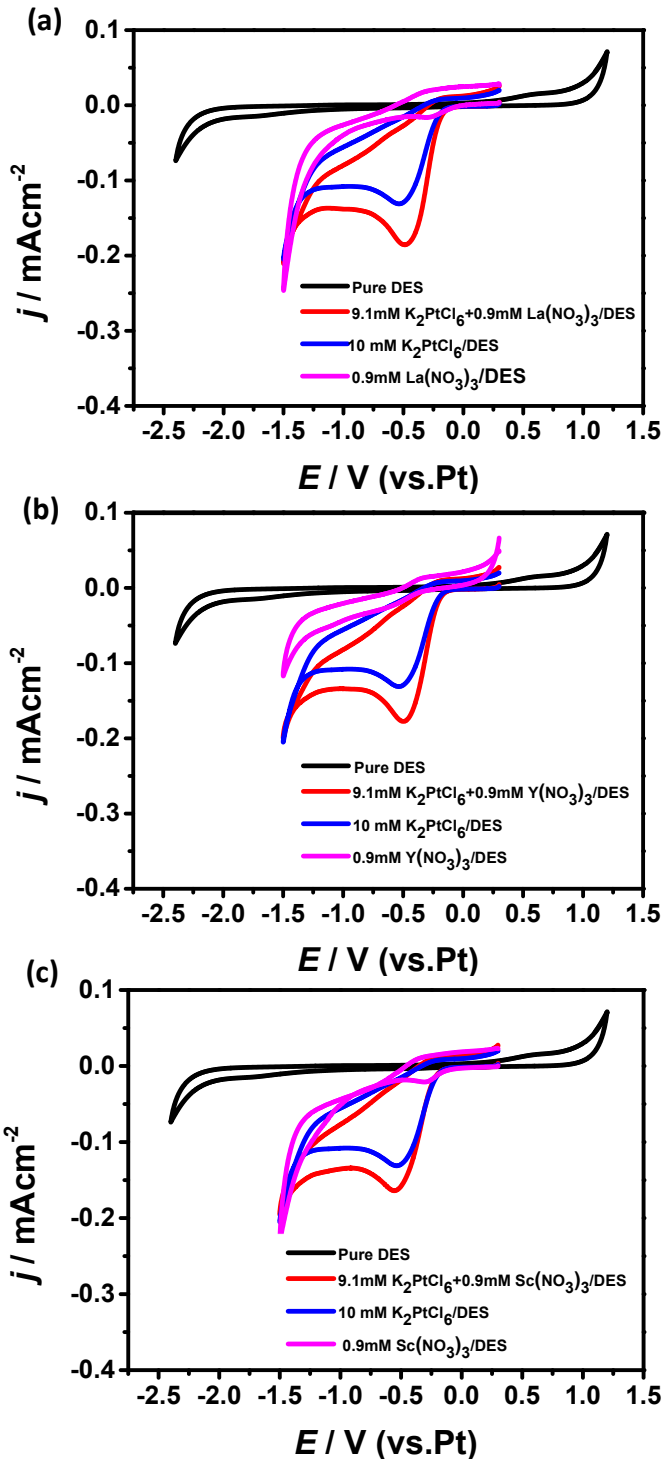

Fig. S1. Cyclic voltammograms recorded on GC electrode in different solutions. Scan rate: 50 mV s^{-1}; Temperature: 80 °C.

Fig. S1(a) exhibits the electrodeposition behaviors of Pt and La. The cyclic voltammograms (CVs) of a GC electrode in the pure choline chloride-urea (ChCl-U) based deep eutectic solvent (DES) (black curve) and ChCl-U based DES solutions containing 0.9 mM $La(NO_3)_3$ (magenta curve), 10 mM K_2PtCl_6 (blue cure) and 9.1 mM K_2PtCl_6 + 0.9 mM $La(NO_3)_3$ (red curve) were performed at a scan rate of 50 mV s^{-1} at 80 ºC. According to the black curve, it can be clearly observed that the ChCl-U based DES exhibits an electrochemical stability window of around 3 V on GC, ranging from –2 V to 1 V with respect to the Pt quasi-reference electrode. The magenta curve shows that there are two cathodic peaks at −0.34 V and −1.25 V, corresponding to La deposition on GC. The distinct reduction process is observed at −0.56 V from the blue curve, which is attributed to the Pt deposition. The red curve was recorded in a ChCl-U based DES solution containing 9.1 mM K_2PtCl_6 and 0.9 Mm $La(NO_3)_3$. It is worth noting that, there yield slightly variation especially for the higher cathodic peak current and more positive cathodic peak potential (−0.55 V), the feature of the CV profile is similar to that obtained in 10 mM K_2PtCl_6 of ChCl-U based DES solution (blue curve). The electrodeposition behaviors of Y and Sc are the same as La, as shown in Fig. S1(b and c). These results indicate that, within the electrochemical stability range of ChCl-U based DES, Pt and RE (RE = La, Y, Sc) are coelectrodeposited and successfully form alloys on the GC electrode without the interference of any electrolyte decomposition reaction.

2. Theoretical values and atomic models of high-index planes

Table S1. The calculated values for the angles of different high-index planes of Miller indices {*hk*0} with the {100} plane.

{*hk*0}	{210}	{310}	{410}	{510}
θ / °	26.56	18.43	14.03	11.31

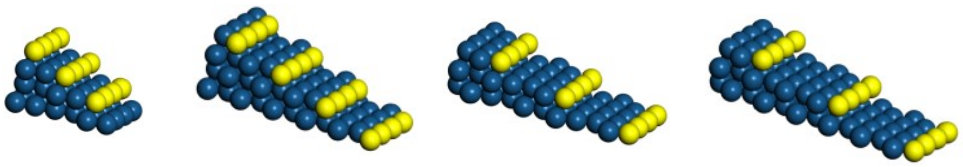

{210} {310} {410} {510}

Fig. S2. Atomic models of high-index {210}, {310}, {410} and {510} planes, respectively.

3. ICP-MS analysis

Table S2. ICP-MS results of as-synthesized Pt-RE (RE = La, Y, Sc) alloys and Pt concave nanocubes.

Samples	Pt	Pt-La		Pt-Y		Pt-Sc	
Elements	Pt	Pt	La	Pt	Y	Pt	Sc
Contents (μg)	0.490	0.598	0.024	0.504	0.091	0.457	0.032
Atomic ratio of Pt/RE	100/0	96/4		98/2		93/7	
Catalyst loading (μg)	0.490	0.622		0.595		0.489	

4. EDX analysis

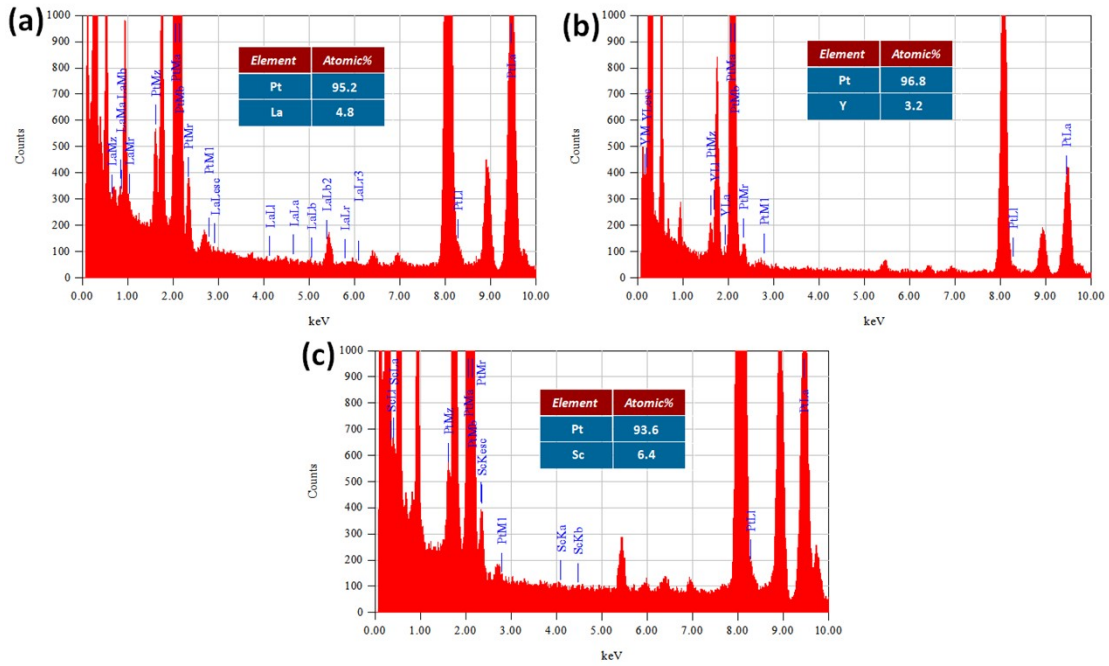

Fig. S3. EDX of the as-prepared PtRENCs: (a) Pt-La, (b) Pt-Y, (c) Pt-Sc.

5. Cyclic voltammograms

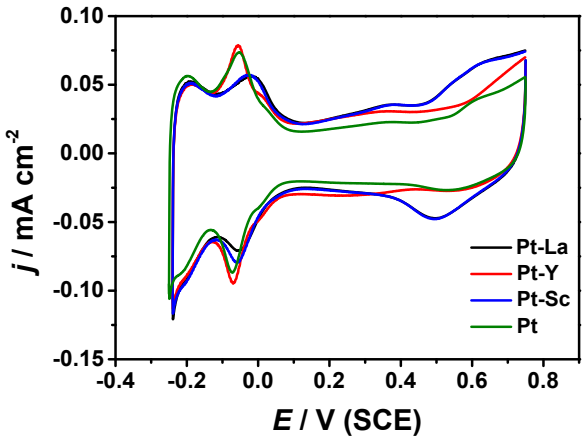

Fig. S4. Cyclic voltammograms of concave cubic Pt-La, Pt-Y, Pt-Sc and Pt NCs in 0.1 M $HClO_4$ solution. Scan rate: 50 mV s^{-1}; temperature: 25 °C.

6. Potentiostatic NRR experiments

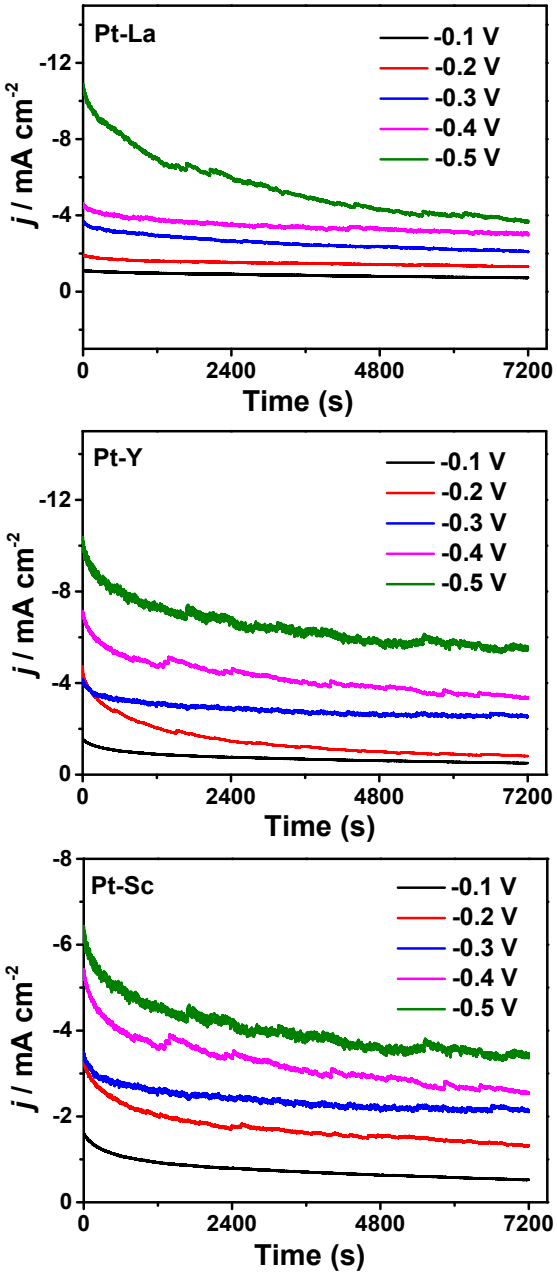

Fig. S5. *i-t* curves of NRR over concave cubic Pt-La, Pt-Y and Pt-Sc alloy NCs in 1 mM HCl solution at different potentials for 2 hr.

7. Calibration curve of NH_4^+ ion concentration

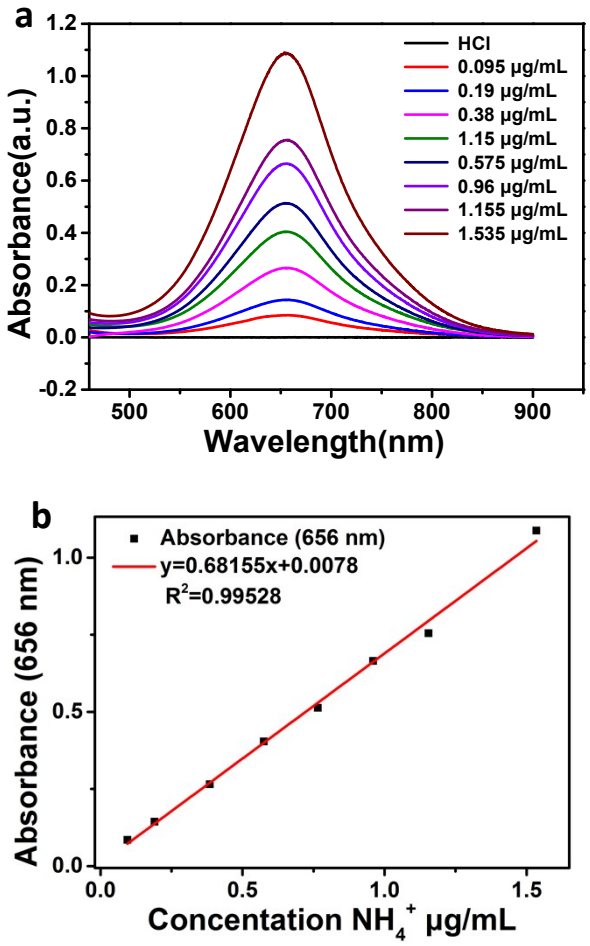

Fig. S6. Absolute calibration of the indophenol blue method using ammonium chloride solutions of known concentration as standards. (a) UV-Vis curves of indophenol assays with NH_4^+ ions after incubated for 1 hour at room temperature; (b) calibration curve used for estimation of NH_3 by NH_4^+ ion concentration. The absorbance at 656 nm was measured by UV-Vis spectrophotometer, and the fitting curve shows good linear relation of absorbance with NH_4^+ ion concentration (y = 0.6815x + 0.0078, R^2 = 0.99528) of three times independent calibration curves.

8. NH_3 yield rates normalized to the electroactive surface areas

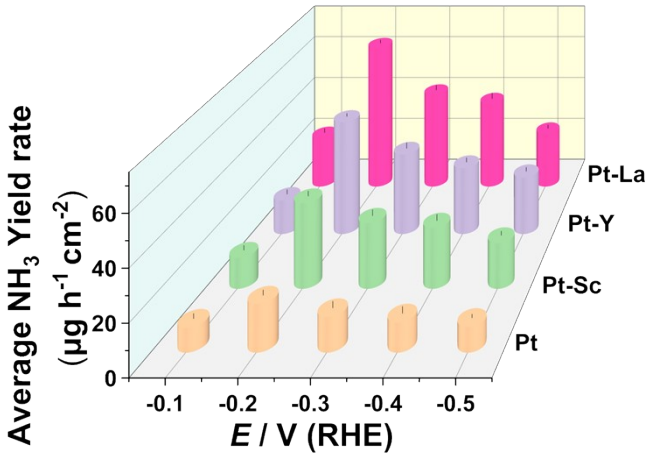

Fig. S7. The NH_3 yield rates of concave cubic Pt-La, Pt-Y, Pt-Sc and Pt NCs at different potentials.

Fig. S7. shows the NH_3 yield rate normalized to the electroactive surface areas, which is calculated by the following equation:

$$r(NH_3) = \frac{[NH_3] \times V}{t \times A}$$

Where A is the electrochemically active surface area, which was calculated from the electric charge of hydrogen adsorption/desorption on catalyst surface.

9. TEM characterization of commercial Pt/C catalyst

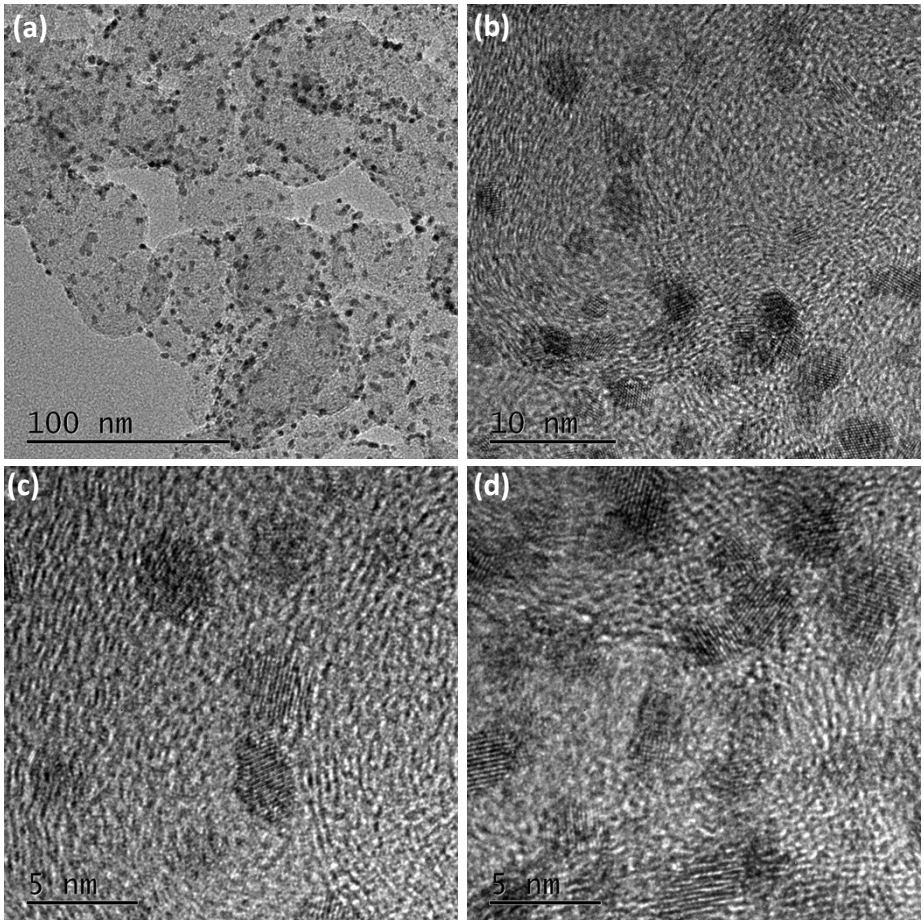

Fig. S8. TEM images of the commercial Pt/C catalyst (20 wt%, Sigmae Aldrich and Alfa Aesar).

10. Comparison of NRR on concave cubic Pt-La alloy NCs, concave cubic Pt NCs and Pt/C catalyst

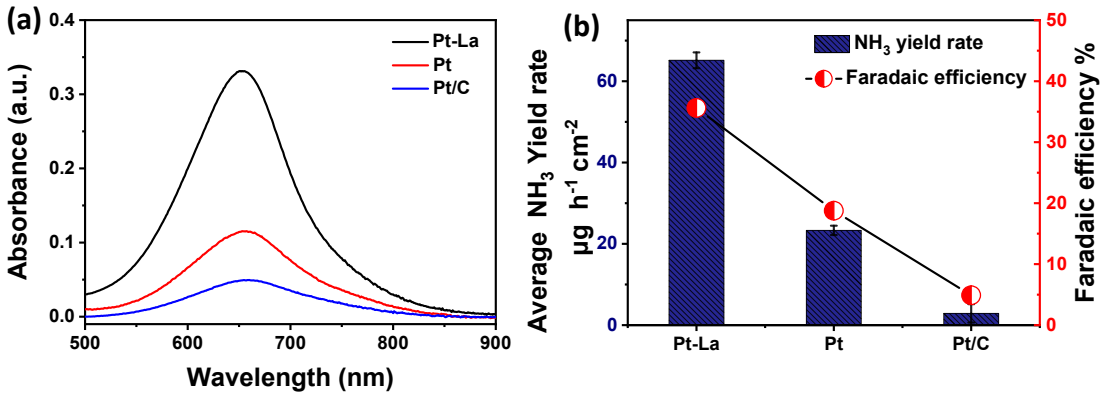

Fig. S9. (a) UV-Vis absorption spectra of the electrolytes stained with indophenol blue indicator after NRR electrolysis on the concave cubic Pt-La alloy NCs, concave cubic Pt NCs and Pt/C catalyst (20 wt%, Sigmae Aldrich and Alfa Aesar)

11. UV-Vis absorption spectra of the electrolytes stained with indophenol blue indicator after NRR electrolysis for different cycling tests

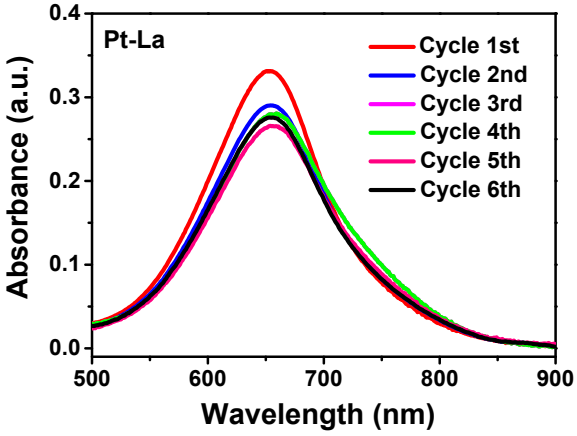

Fig. S10. UV-Vis absorption spectra of the electrolytes stained with indophenol blue indicator after NRR electrolysis on the concave cubic Pt-La alloy NCs in 1 mM HCl solution for different cycling tests.

12. long-term chronoamperometric test

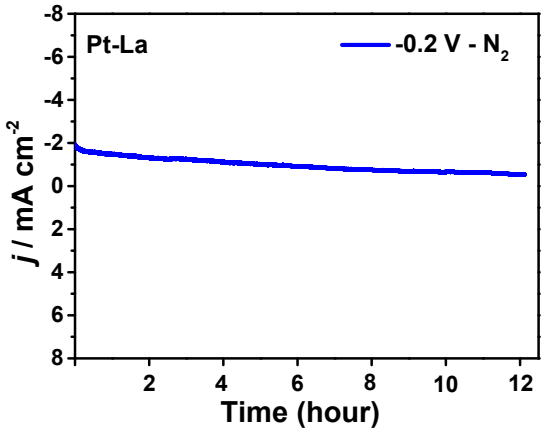

Fig. S11. *i-t* curves of NRR over concave cubic Pt-La alloy NCs in 1 mM HCl solution at different potentials for 12 hr.

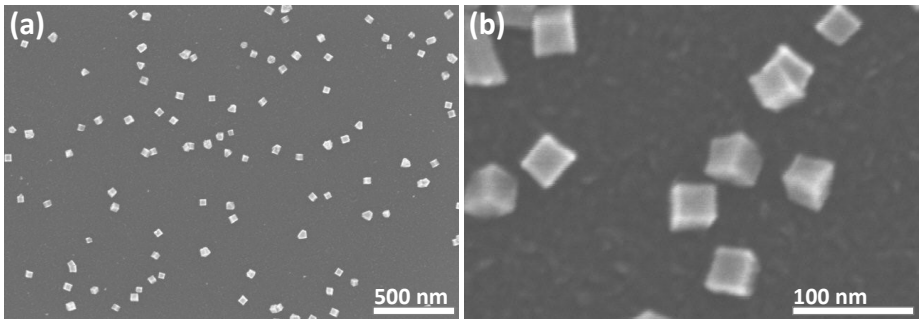

Fig. S12. SEM image of the concave cubic Pt-La alloy NCs obtained after NRR endurance cycle test, confirming that the Pt-La alloy NCs still kept the concave cubic shape after the reaction.

13. UV-vis absorption spectra of the electrolytes stained with Watt-Chrisp methods

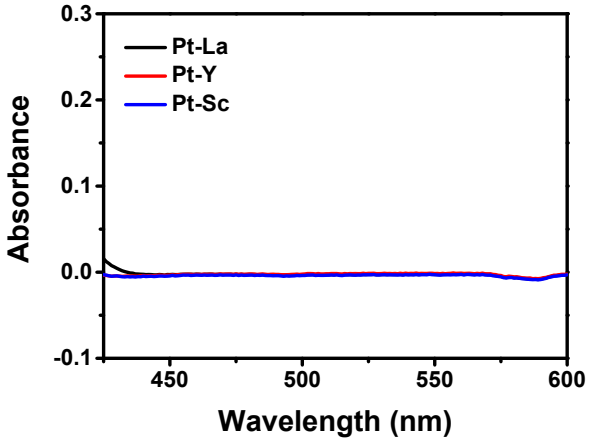

Fig. S13. UV-vis absorption spectra of the electrolytes stained with Watt-Chrisp methods after NRR electrolysis on concave cubic Pt-La, Pt-Y and Pt-Sc alloy NCs at -0.4 V for 2 hr.

14. Quantitative analysis of $^{15}NH_3$ by ^{1}H NMR

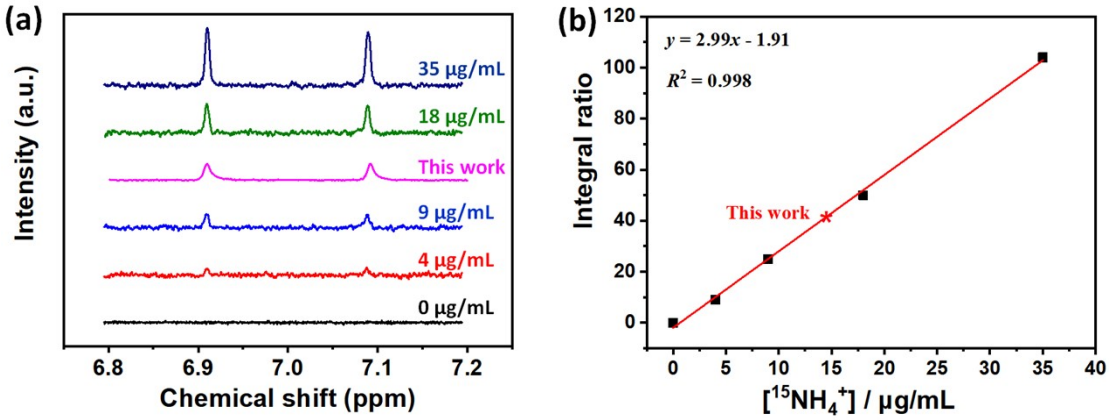

Fig. S14. (a) ^{1}H NMR analysis of $^{15}NH_4Cl$ standard solutions, and (b) ^{1}H NMR calibration plots for the quantification of $^{15}NH_4^+$.

15. XPS survey spectra

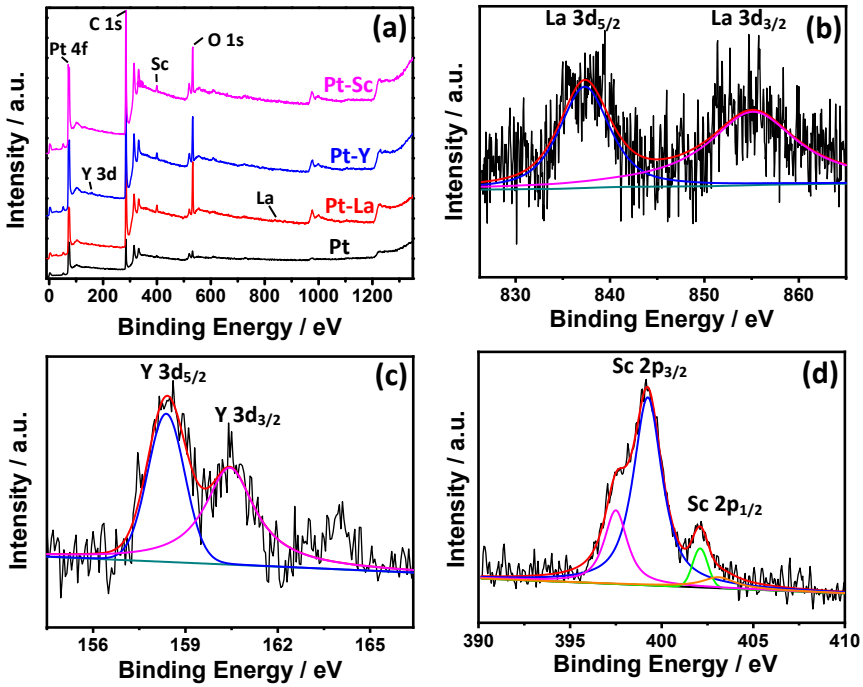

Fig. S15. (a) XPS survey spectra of concave cubic Pt, Pt-La, Pt-Y and Pt-Sc NCs. High resolution La 3d (b), Y 3d (c) and Sc 2p (d) spectra of Pt-La, Pt-Y and Pt-Sc samples, respectively.

16. Computational methods

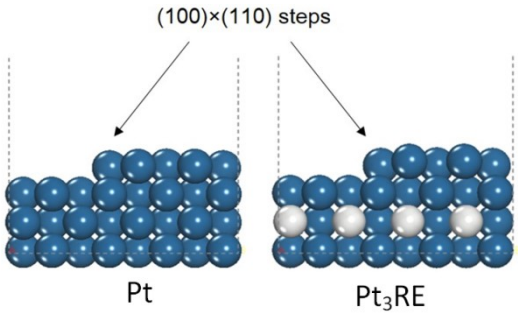

Fig. S16. Side views of theoretical models of (100)×(110) steps on Pt and Pt_3RE (RE = La, Y, Sc). Blue: Pt; silver: RE (RE = La, Y, Sc). Dashed grey lines indicate the periodical boundaries.

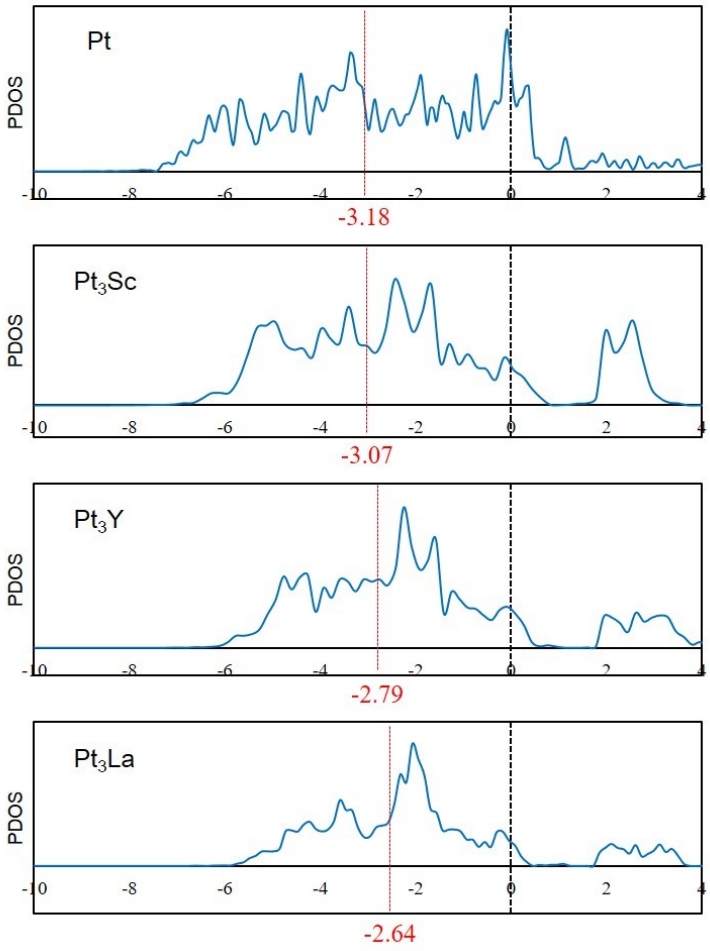

Fig. S17. Calculated d-projected density of states of the Pt atoms in bulk Pt and Pt_3RE (RE = La, Y, Sc). The Fermi level has been set to zero as shown in black dashed lines. The red dashed lines indicates the positions of d-band centres.

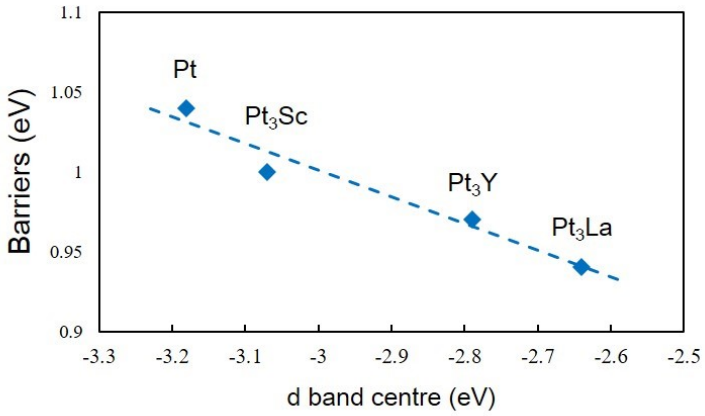

Fig. S18. The linear relations between d-band centres of the Pt atoms in bulk Pt and Pt_3RE (RE = La, Y, Sc) and the overall barriers in nitrogen reduction reactions.

Table S3. Calculated Gibbs free reaction energies (unit in eV) of elementary steps for nitrogen reduction reactions at steps on Pt and Pt_3RE (RE = La, Y, Sc) respectively.

reactions	Pt	Pt_3Sc	Pt_3Y	Pt_3La
$N_2 + H^+ + e^- \rightarrow N_2H^*$	0.87	0.86	0.84	0.81
$N_2H^* + H^+ + e^- \rightarrow N_2H_2^*$	0.17	0.14	0.13	0.13
$N_2H_2^* \rightarrow 2NH^*$	-0.30	-0.97	-0.98	-0.99
$NH^* + H^+ + e^- \rightarrow NH_2^*$	-0.53	-0.40	-0.39	-0.39
$NH_2^* + H^+ + e^- \rightarrow NH_3$	-0.05	0.19	0.20	0.22

Table S4. Calculated d-band centres (unit in eV) of the Pt atoms in bulk Pt and Pt_3RE (RE = La, Y, Sc) and the overall barriers (unit in eV) in nitrogen reduction reactions.

	Pt	Pt_3Sc	Pt_3Y	Pt_3La
d-band centres	-3.18	-3.07	-2.79	-2.64
overall barriers	1.04	1.00	0.97	0.94

17. Hydrogen evolution reaction (HER): Experimental and computational

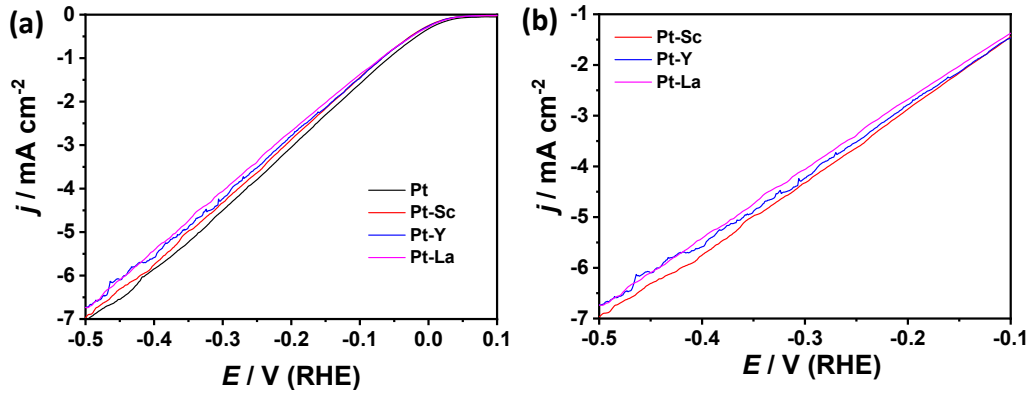

Fig. S19. (a) LSV curves of monometallic Pt and Pt-RE (RE = La, Y, Sc) alloy concave nanocubes in Ar-saturated 1 mM HCl solution with a scan rate of 10 mV s^{-1}. (b) LSV curves of Pt-RE (RE = La, Y, Sc) alloy concave nanocubes between the potential range from –0.10 and –0.50 V (RHE).

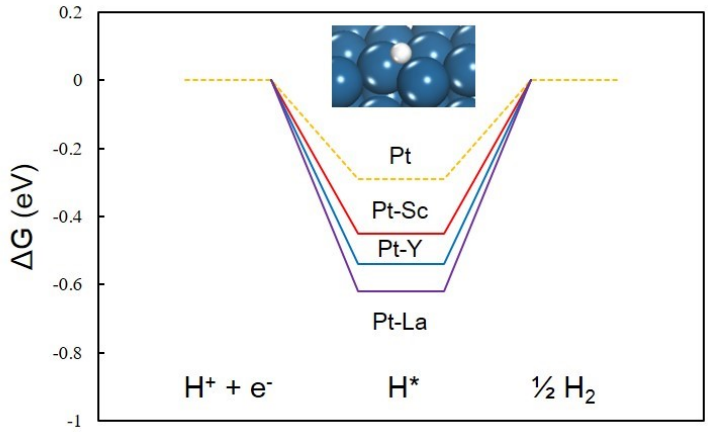

Fig. S20. Free energy profiles for HER at steps on Pt and Pt-RE (RE = La, Y, Sc) under the standard hydrogen electrodes condition, $U = 0$ V vs SHE.

Fig. S19(a) shows LSV curves of monometallic Pt and Pt-RE (RE = La, Y, Sc) alloy concave nanocubes in Ar-saturated 1 mM HCl solution, indicating that the introduction of RE (RE = La, Y, Sc) on Pt step surface can effectively suppress the HER. Particularly, the suppression effect is in the order of La > Y > Sc between the potential range from –0.10 and –0.50 V (RHE) (Fig. S19(b)), which were applied to NRR electrolysis on PtRENCs. We further carried out density functional theory

(DFT) calculations of the binding energy of H* which was suggested as a crucial descriptor for HER activity according to the Sabatier's rules; the value of H* binding energy closer to zero indicates the higher activity. The H* binding energy at steps gives the order: Pt-La (-0.62 eV) < Pt-Y (-0.54 eV) < Pt-Sc (-0.45 eV) < Pt (-0.29 eV), indicating that the HER activity would be suppressed thus giving a higher FE with the order of Pt-La > Pt-Y > Pt-Sc > Pt (Fig. S20).